Inelastic deformation of metallic glasses under dynamic cyclic loading

Y.J. Duan [a,b], J.C. Qiao [a,*], T. Wada [c], H. Kato [c], Y.J. Wang [d,e], E. Pineda [b], D. Crespo [b]

[a] *School of Mechanics, Civil Engineering and Architecture, Northwestern Polytechnical University, Xi'an 710072, China*
[b] *Department of Physics, Institute of Energy Technologies, Universitat Politècnica de Catalunya, Barcelona 08019, Spain*
[c] *Institute for Materials Research, Tohoku University, Sendai 980-8577, Japan*
[d] *State Key Laboratory of Nonlinear Mechanics, Institute of Mechanics, Chinese Academy of Sciences, Beijing 100190, China*
[e] *School of Engineering Science, University of Chinese Academy of Sciences, Beijing 101408, China*

ARTICLE INFO

ABSTRACT

Dynamic mechanical analysis was performed in two metallic glasses that show markedly distinct β relaxation features. The confined flow defects of free-volume zones and the inelastic deformation behavior result into a significant mechanical hysteresis loop in dynamic cyclic loadings, which is described with a viscoelastic model. Annealing below the glass transition temperature T_g decreases the concentration of free-volume zones. The understanding of the inelastic deformation, which is related to free-volume zones, is critical and may provide a new avenue into the mechanical properties' improvement of high entropy metallic glasses.

© 2020 Acta Materialia Inc. Published by Elsevier Ltd. All rights reserved.

Metallic glasses (MGs) and high-entropy alloys (HEAs) have stimulated tremendous research interest in both material science and condensed matter physics for decades [1–6]. More recently, high-entropy metallic glasses (HE-MGs) have been developed overlapping the definitions of both MGs and HEAs [7–9]. Compared with the conventional MGs, HE-MGs exhibit unique mechanical properties (i.e. excellent strength at ambient temperature) [9–12]. As a consequence, HE-MGs provide a new avenue to develop new materials for functional and structural applications. Large experimental [13,14], theoretical [5,6,15] and numerical simulation [13] efforts explored the nature of atomic-scale structures in MGs, and the connection between these microscopic structures and the mechanical response of amorphous alloys. However, it is still a challenging issue to fully understand the link between the atomic-scale disordered structure and mechanical deformation behavior in MGs, in analogy to the scenario of crystalline defects in crystals, especially in the recently emerging HE-MGs [16–18].

It is known that MGs show both elasticity and viscoelasticity and that fluctuation in the excess free-volume generates the so-called "soft" spots surrounded by a stiffer elastic matrix [19–21]. However, the mechanical properties of these high free-volume regions are not thoroughly understood up to date. Besides, a comprehensive understanding of the interplay between the free-volume zones and the elastic matrix, as well as the relationship with the

macroscopic mechanical properties, is still lacking. The comprehension of such mechanics may provide new tools for the improvement of the mechanical properties of MGs. In the current work, a $Pd_{20}Pt_{20}Cu_{20}Ni_{20}P_{20}$ HE-MG and a $La_{60}Ni_{15}Al_{25}$ MG, with distinct β relaxation responses, are chosen as model alloys to prove and quantify the flow defects and inelastic deformation behaviors under dynamic cyclic loading. An interesting hysteresis loop phenomenon was found and it is rationalized in the framework of a viscoelastic model.

Due to the extremely high thermal stability and outstanding glass forming ability (GFA) [22], $Pd_{20}Pt_{20}Cu_{20}Ni_{20}P_{20}$ HE-MG was selected. $La_{60}Ni_{15}Al_{25}$ is a regular metallic glass with a distinct β relaxation. The thermal properties of both alloys were determined by differential scanning calorimetry (DSC, Netzsch 202). The glass transition temperature T_g and the onset crystallization temperature T_x were determined and are shown in Fig. 1(a), respectively.

Dynamic Mechanical Analysis provides a way to investigate the relaxation processes originated by atomic/molecular rearrangements in glassy solids (e.g. polymers or metallic glasses) [4,23]. The temperature dependences of the storage modulus E'/E_u and the loss modulus E''/E_u of $Pd_{20}Pt_{20}Cu_{20}Ni_{20}P_{20}$ are shown in Fig. 1(b), E_u being the value of the storage modulus at room temperature. The following remarkable features can be noticed. (I) The loss modulus E''/E_u shows a shoulder and a distinct peak: the shoulder at lower temperature (520 K) is identified as β relaxation while the distinct peak at higher temperature (580 K) corresponds to the α relaxation. (II) The intensity of the shoulder (β relaxation) is lower than that of the peak of α relaxation. (III)

---

* Corresponding author.
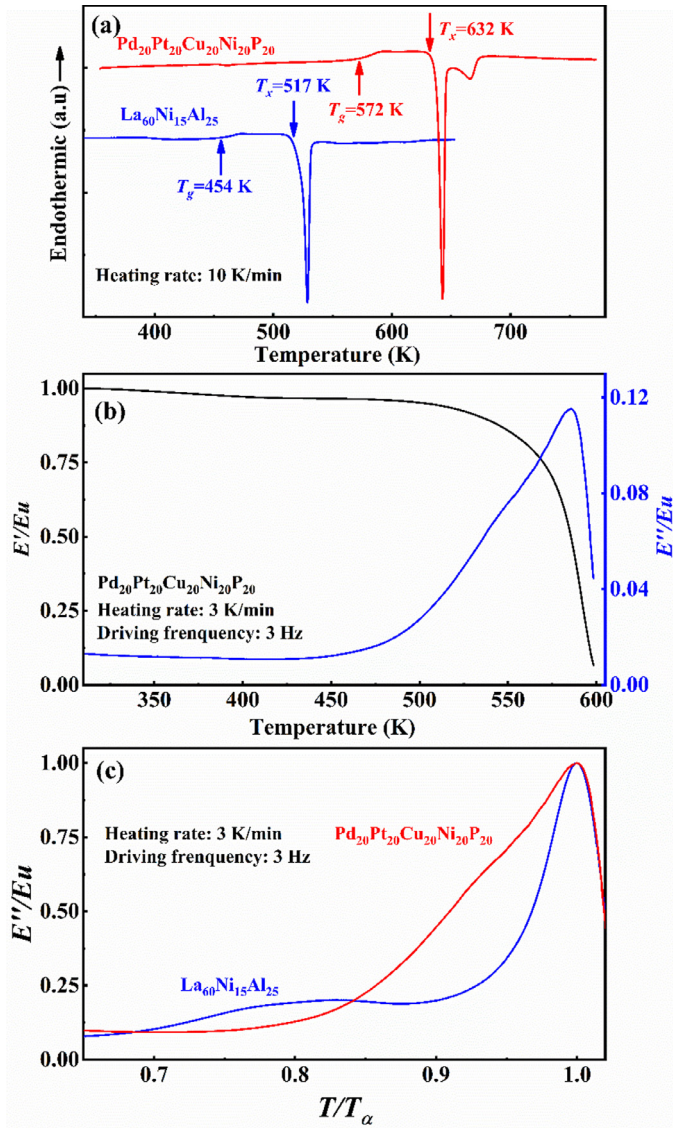*E-mail address:* qjczy@nwpu.edu.cn (J.C. Qiao).

Fig. 1. (a) DSC curves of $Pd_{20}Pt_{20}Cu_{20}Ni_{20}P_{20}$ and $La_{60}Ni_{15}Al_{25}$. (b) Normalized storage modulus E'/E_u and loss modulus E''/E_u of $Pd_{20}Pt_{20}Cu_{20}Ni_{20}P_{20}$ versus temperature. E_u is the initial value of the storage modulus at ambient temperature. (c) The normalized loss modulus E''/E_u of both $Pd_{20}Pt_{20}Cu_{20}Ni_{20}P_{20}$ and $La_{60}Ni_{15}Al_{25}$ against the normalized temperature T/T_a.

Compared with the change of loss modulus, E''/E_u, the storage modulus E'/E_u shows a large drop at the temperature corresponding to the α relaxation. Previous literature showed that the α relaxation and β relaxation processes provide important insight into the glass transition behavior, plasticity, and mechanical dynamics of MGs [4,24,25]. The intensity of the β relaxations accounts for the microscopic motion of atoms. As shown in Fig. 1(c), $La_{60}Ni_{15}Al_{25}$ shows a distinct slow β relaxation peak, while $Pd_{20}Pt_{20}Cu_{20}Ni_{20}P_{20}$ exhibits a noticeable shoulder. The α relaxation links to a thermodynamically irreversible process, corresponding to the large-scale collective rearrangement of atoms above the dynamic glass transition. However, the β relaxation is a reversible process, which is related to a series of localized flow defects in free-volume zones, being dispersed in an elastic amorphous matrix [19].

The stress-strain curves of $Pd_{20}Pt_{20}Cu_{20}Ni_{20}P_{20}$ and $La_{60}Ni_{15}Al_{25}$ at $0.87T_g$ are shown in Fig. 2(a). The ultimate stress of $Pd_{20}Pt_{20}Cu_{20}Ni_{20}P_{20}$ is ~2.6 times higher than that of $La_{60}Ni_{15}Al_{25}$. The experimental results of the dynamic cyclic

loading test on $La_{60}Ni_{15}Al_{25}$ (only the first four cycles) are shown in Fig. 2(b). The dynamic cyclic loading tests of ten cycles of $La_{60}Ni_{15}Al_{15}$ and $Pd_{20}Pt_{20}Cu_{20}Ni_{20}P_{20}$ with maximum stress of $0.7\sigma_u$ are further shown in Fig. 2(c) and (d), respectively. It is noted that the mechanical hysteresis loops reduce largely in successive dynamic cycles. Fig. 3 shows the first cycle of the inelastic deformation of (a) $La_{60}Ni_{15}Al_{25}$ and (b) $Pd_{20}Pt_{20}Cu_{20}Ni_{20}P_{20}$ with different magnitude of maximum stress. The effect of annealing is shown in Fig. 3(c) and (d). As the maximum stress increases, the mechanical hysteresis loops expand strikingly as shown in Fig. 3(a) and (b). The residual displacements after cyclic loading, shown in Fig. 3(a)–(d), result from the dynamic response of the inelastic deformation.

The mechanical hysteresis loops unambiguously confirm that the flow defects in the soft free-volume zones become activated even at a stress far less than the yield strength. The atomic motion dissipates the strain energy during cyclic loading, confirming that the deformation within the elastic regime of the MGs is viscoelastic. The activated flow defects in soft free-volume zones contribute to the mechanical hysteresis loop of the MGs [26–28]. The markedly different viscoelastic behavior under different stress levels and sample states are shown in Fig. 3(a)–(d). The hysteresis loop of $Pd_{20}Pt_{20}Cu_{20}Ni_{20}P_{20}$ is obviously larger than that of $La_{60}Ni_{15}Al_{25}$, indicating that the viscosities of the flow defects at the same relative temperature of $0.87T_g$ are different in the MG and the HE-MG.

To quantify the loss of energy in each cycle we define $\Delta W = W_1 - W_2$, where W_1, W_2 are defined as the area under the stress–strain curve during the loading and unloading stages, respectively. Both the residual strain $\Delta\varepsilon$ (after a complete loading–unloading period) and the loss energy factor $\dot{W} = \frac{\Delta W}{W_1}$ increase as the maximum stress increases in $Pd_{20}Pt_{20}Cu_{20}Ni_{20}P_{20}$ – Fig. 4(a) –, while those of $La_{60}Ni_{15}Al_{25}$ show little changes – Fig. 4(b) –. This indicates that the increase of the maximum stress enhances very differently the inelastic deformation in MGs depending on the alloy. Furthermore, the hysteresis loop expands conspicuously with the increase of the maximum stress, as shown by the dynamic cyclic loading, implying an excellent damping ability of MGs at high temperatures, as derived from their high loss energy factor.

It has long been considered that flow defects in free-volume zones can be regarded as regions with 'liquid-like' atoms [29,30], thus resulting in structural heterogeneities which can accommodate deformation under an applied load. On the basis of the present results [15,19,31] the flow defects in free-volume zones can be thought of as loosely packed regions caged in the hard elastic surroundings. Egami et al. reported that the increase in the number of free-volume zones in MGs is due to the change of the distribution of atomic level stresses in MGs [32,33]. The "core-shell" model, consisting of free-volume rich zones in an elastic matrix, describes the basic features of the atomic structure of MG, as schematically shown in Fig. 3(e). To understand the details of the activation process of the flow defects and the inelastic behavior of MGs, a Kelvin-type viscoelastic model is proposed. The model describes the free-volume zones as a fluid with an effective viscosity η_{eff}, obeying Newtonian flow, and the elastic surroundings as a solid with an effective modulus E_{eff}. These elements are shown as a dashpot and an elastic spring, respectively, connected in parallel as illustrated in Fig. 3(f). The viscoelastic response of such a system is expressed as

$$\sigma = E_{eff}\varepsilon + \eta_{eff}\frac{d\varepsilon}{dt}, \tag{1}$$

where σ and ε are the applied stress and the observed strain. The effective relaxation time is defined as $\tau_{eff} = \frac{\eta_{eff}}{E_{eff}}$, which can be compared to the strain rate $\dot{\varepsilon}$ which acts as characteristic deformation time by defining the dimensionless parameter $\delta_{eff} = \frac{\eta_{eff}}{E_{eff}} \cdot \dot{\varepsilon}$.
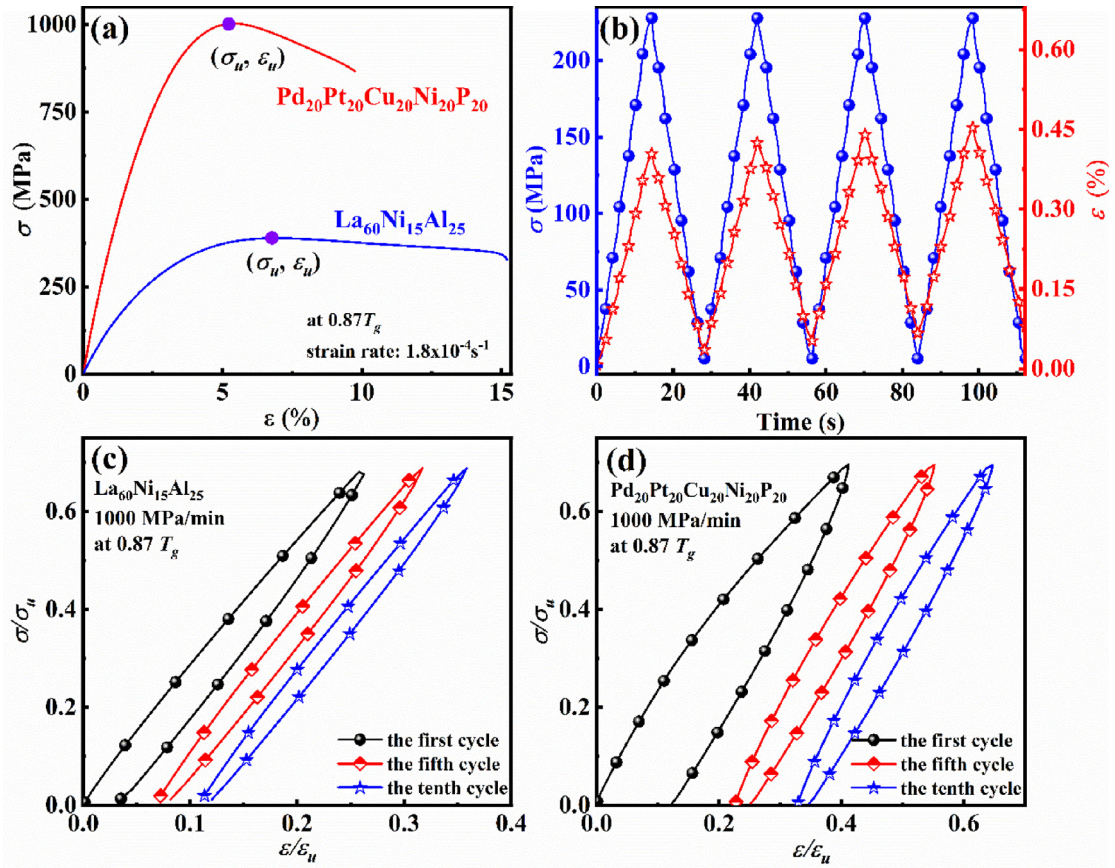
Fig. 2. (a) The tensile stress–strain curves of $Pd_{20}Pt_{20}Cu_{20}Ni_{20}P_{20}$ and $La_{60}Ni_{15}Al_{25}$ at $0.87T_g$. (b) The $La_{60}Ni_{15}Al_{15}$ stress and strain values during the loading–unloading cycles with a maximum stress level of $0.6\sigma_u$ (only the first four cycles are shown). Dynamic cyclic loading tests of first, fifth and tenth cycle of (c) $La_{60}Ni_{15}Al_{15}$ and (d) $Pd_{20}Pt_{20}Cu_{20}Ni_{20}P_{20}$ with different maximum stress of $0.7\sigma_u$ at $0.87T_g$.

The parameters of the viscoelastic model in Eq. (1) can be computed in an iterative manner by fitting the experimental data. The results in Fig. 4(c) show that the effective viscosity η_{eff} of $Pd_{20}Pt_{20}Cu_{20}Ni_{20}P_{20}$ and $La_{60}Ni_{15}Al_{25}$ increases as the maximum stress increases. Contrarily, the effective modulus E_{eff} shows little change for both MGs, as shown in Fig. 4(d). The obtained average viscosity η_{eff} of $Pd_{20}Pt_{20}Cu_{20}Ni_{20}P_{20}$ is ~12 times higher than that of $La_{60}Ni_{15}Al_{25}$, while the average modulus E_{eff} of $Pd_{20}Pt_{20}Cu_{20}Ni_{20}P_{20}$ is only about twice that of $La_{60}Ni_{15}Al_{25}$. The most interesting phenomenon is the behavior of the effective relaxation times τ_{eff} and the parameter δ_{eff} in Fig. 4(e) and (f). The relaxation time of $Pd_{20}Pt_{20}Cu_{20}Ni_{20}P_{20}$ is ~7 times higher than that of $La_{60}Ni_{15}Al_{25}$ due to the sluggish diffusion of HE-MG. More interestingly, δ_{eff} has a similar value in both alloys for the low maximum applied stresses, but increases largely in the HE-MG while remains quite constant in the La-based MG. The increase of δ_{eff} in the HE-MG is a consequence of the strain hardening observed as the maximum stress increases, responsible for the increasing loss energy factor $\dot{W}$ shown in Fig. 4(b). The lower atomic diffusivity of the HE-MG severely restrains the strain both in the load and unload phase, being responsible also for the increasing residual strain – Fig. 4(a) – as the maximum applied stress increases. The distinct viscosity and relaxation time appear to be responsible for the obviously different hysteresis loop between the HE-MG and the MG. As we know, the high mixing entropy of HE-MG is beneficial to reduce the Gibbs free energy [34]. Specifically, the sluggish diffusion of HE-MG significantly hinders the atomic mobility [35].

Due to the difficulty to describe structural features in MGs during dynamic cyclic loading, the discussion on the inelastic defor-

mation mechanism of MGs is still under debate. Therefore, the commonly accepted theoretical description is used here to explain these mechanistic processes. The distribution of the flow units (or soft spots) in MGs is affected by the chemical composition and the glass transition temperature T_g. The above model should be modified such that it includes the viscoelastic flow defects with an effective viscosity η_{eff} and the elastic matrix with an effective modulus E_{eff}. When dynamic cyclic loading is applied on MGs, a certain fraction of the flow units is activated in each cycle, and the rest of the material acts as an elastic matrix. The structures of both HE-MGs and MGs will be changed after successive cycles. Therefore, there will be more probability in the next cycles to nucleate new excitation from the vicinity of a previous flow defect, because the previous one has been rejuvenated and was driven to a unstable, high-energy level. This scenario is evidenced by the fact that both the effective modulus E_{eff} and obtained average viscosity η_{eff} decrease after successive dynamic cycles, as shown in Fig. S1 (c) and (d) in Supplementary Materials. This observation is in agreement with molecular dynamics simulations that cyclic loading induces structural, mechanical, and energetic rejuvenation in MG [36]. The residual strain $\Delta\varepsilon$ accumulated after each cycle in both $Pd_{20}Pt_{20}Cu_{20}Ni_{20}P_{20}$ HE-MG and $La_{60}Ni_{15}Al_{25}$ MG, as shown in Fig. S1 (a) in Supplementary Materials, as a result of this softening process. De Hosson reported similar results under cycle compression of $Al_{86}Ni_9Y_5$ MG [21]. The physical explanation for the residual strain accumulation under dynamic cycles comes from the visco-elastic component of the constitutive model. The initial elastic deformation of the MG structure becomes irreversible as the elapsed time becomes comparable to the relaxation time, allowing the structural excitation or viscoelastic deformation of flow-defect
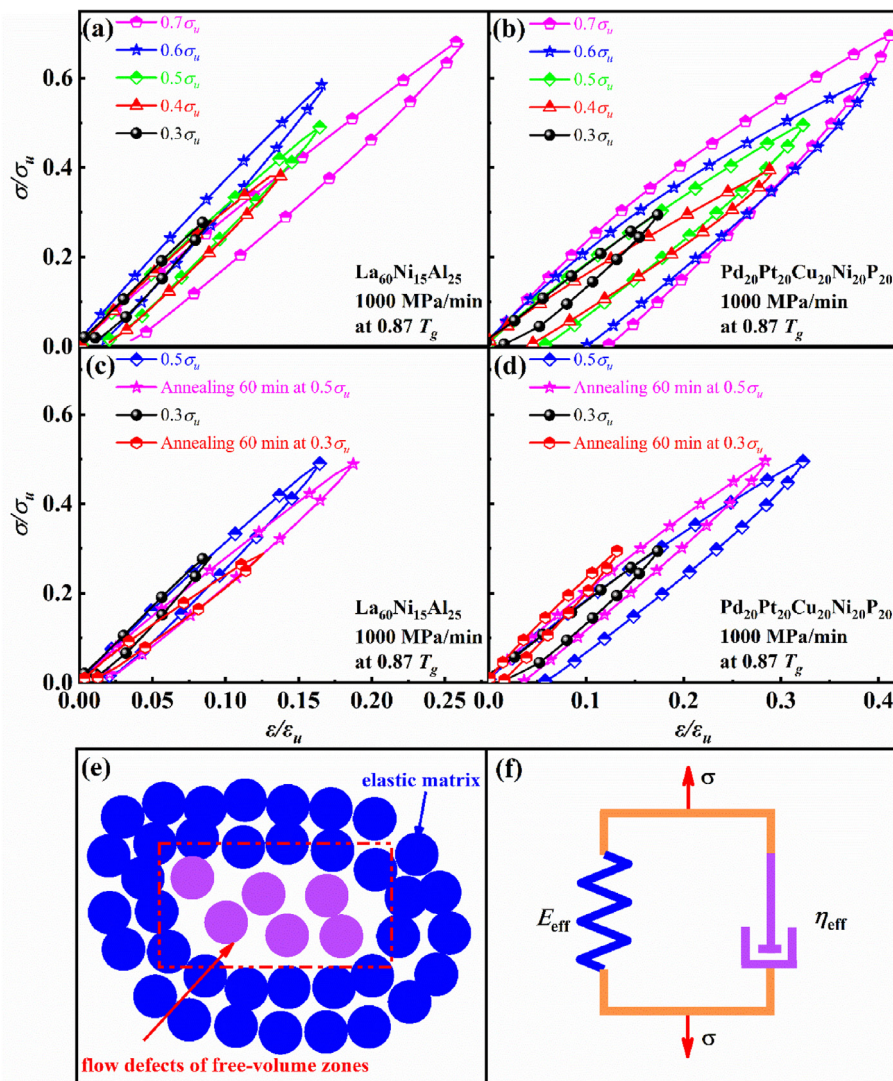
Fig. 3. Dynamic cyclic loading tests of first cycle of (a) La$_{60}$Ni$_{15}$Al$_{25}$ and (b) Pd$_{20}$Pt$_{20}$Cu$_{20}$Ni$_{20}$P$_{20}$ with different maximum stress at 0.87T_g. Evolution of the stress–strain curves of the as-cast sample and sample annealed at 0.87T_g for 60 min of (c) La$_{60}$Ni$_{15}$Al$_{25}$ MG and (d) Pd$_{20}$Pt$_{20}$Cu$_{20}$Ni$_{20}$P$_{20}$ HE-MG. (e) The "core-shell" model of MG consisting of free-volume zones surrounded by the elastic matrix. (f) A Kelvin-type viscoelastic model.

zones. Therefore, the residual strain accumulates and the softening occurs in both HE-MGs and MGs.

The mechanical and physical properties of MGs also show a strong dependence on physical aging below T_g. Annealing can tailor the elastic modulus, relaxation enthalpy and other mechanical properties in MGs [3,20]. The dependence of the flow defects in free-volume zones on the annealing time was tested, and it is shown in Fig. 3(c) and (d). Taking the as-cast state as reference state, the residual strain $\Delta\varepsilon$ decreases after annealing at the applied stress of 0.5σ_y for Pd$_{20}$Pt$_{20}$Cu$_{20}$Ni$_{20}$P$_{20}$, as shown in Fig. 4(g). However, there is almost no change on the residual strain for La$_{60}$Ni$_{15}$Al$_{25}$. Below T_g, annealing drives MGs towards a more stable state than the reference state of the as-cast samples [37]. Furthermore, annealing below T_g induces a better atomic packing, shortening the interatomic distances. All these factors contribute to the decrease in the concentration of flow defects in both HE-MGs and MGs after annealing. This is supported by the previous findings that the structural homogeneity in both HE-MGs and MGs increased by annealing below T_g [38]. Li et al. reported that the concentration of flow defects in glass by annealing, which results in the embrittlement of the alloy [18,39]. Furthermore, Brechtl et al. [20] found that annealing after irradia-

tion largely affects the atomic disordering, and causing increase in hardness and modulus of BMGs. Thus, annealing of both HE-MGs and MGs leads to the thermal annihilation of flow defects. Therefore, the loss energy factor $\dot{W}$ decreases for the annealed samples of La$_{60}$Ni$_{15}$Al$_{25}$ and Pd$_{20}$Pt$_{20}$Cu$_{20}$Ni$_{20}$P$_{20}$, such change being larger for the Pd-based than for the La-based alloy as shown in Fig. 4(h). The important differences of the aging effects on the cyclic loading behavior between the two alloys could be associated to the very distinct features of their relaxation spectra in Fig. 1(b) and (c). The mechanical processing (i.e. inelastic deformation under dynamic cyclic loading) of as-cast samples activates a larger amount of flow defects, leading to an obvious increase of residual strain and a larger loss energy factor $\dot{W}$.

In summary, the residual strain and the loss energy factor of a high-entropy Pd$_{20}$Pt$_{20}$Cu$_{20}$Ni$_{20}$P$_{20}$ amorphous alloy and a conventional La$_{60}$Ni$_{15}$Al$_{25}$ MG are characterized by dynamic cyclic loading. An interesting mechanical hysteresis loop phenomenon is revealed. The inelastic deformation behavior of the mechanical hysteresis loop is proved and quantified. Annealing below T_g increases the atomic packing density of the atomic structures and decreases the concentration of flow defects related to free-volume zones. The experimental hysteresis loop is described in the framework of a
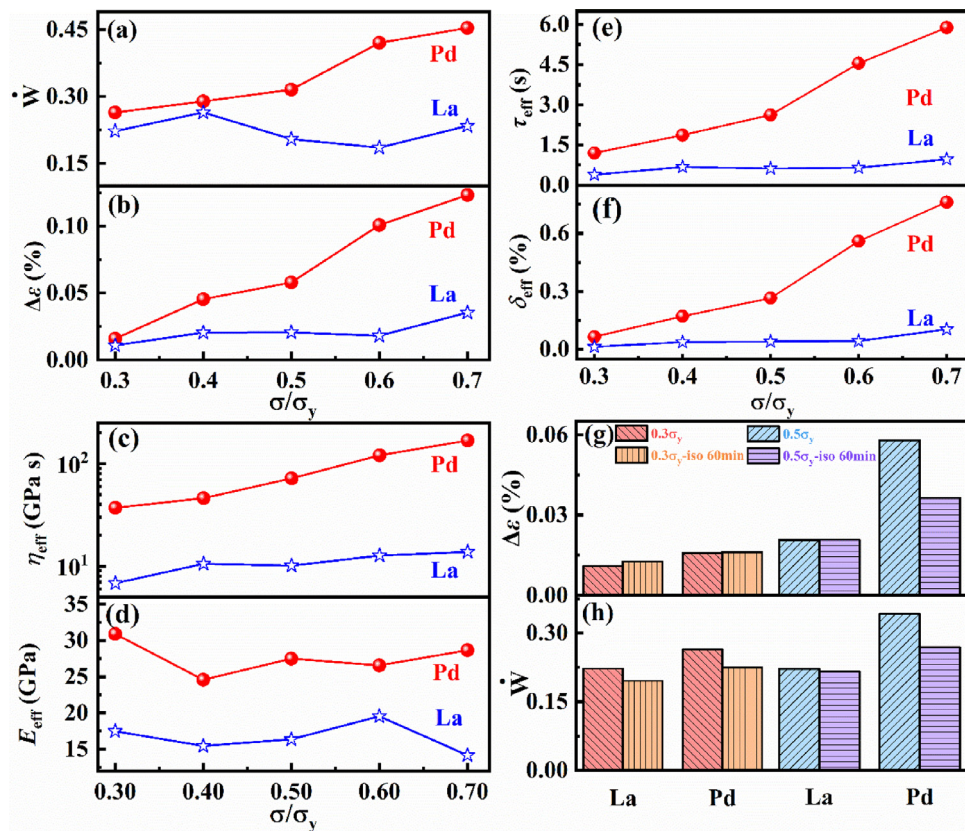
Fig. 4. (a) The loss energy factor $\dot{W}$ and (b) the residual strain of both alloys at different maximum stress at $0.87T_g$ of first cycle. (c) The effective viscosity η_{eff} and (d) the effective modulus E_{eff} in the viscoelastic model. (e) The effective relaxation time τ_{eff} and (f) the dimensionless parameter δ_{eff} of both alloys. (g) The residual strain and (h) the loss energy factor $\dot{W}$ of both alloys with different sample status (as-cast sample or annealing sample) at $0.87T_g$.

viscoelastic model, revealing strain softening after successive dynamic cycles of the HEA alloy. The experimental results provide insight into the inelastic deformation accommodated by the motion of flow defects of free-volume zones in both the HE-MG and the MG. By comparison of the two distinct amorphous alloys, the role of high mixing entropy in the inelastic deformation of MGs is discussed by analyzing the hysteresis loop during cyclic loadings.

Declaration of Competing Interest

None.

Supplementary materials

Supplementary material associated with this article can be found, in the online version, at doi:10.1016/j.scriptamat.2020.113675.

References

[1] W.K. Klement, R.H. Willens, P. Duwez, Nature 187 (4740) (1960) 869–870.
[2] W. Dmowski, T. Iwashita, C.-.P. Chuang, J. Aimer, T. Egami, Phys. Rev. Lett. 105 (20) (2010) 205502.
[3] W.H. Wang, Prog. Mater. Sci. 57 (3) (2012) 487–656.
[4] W.H. Wang, Prog. Mater. Sci. 106 (2019) 100561.
[5] F. Spaepen, Acta Metall. 25 (4) (1977) 407–415.
[6] D.B. Miracle, Nat. Mater. 3 (10) (2004) 697–702.
[7] E. Goncharova, R. Konchakov, A. Makarov, N. Kobelev, V. Khonik, J. Phys. – Condens. Mater. 29 (30) (2017) 305701.
[8] M.W. Glasscott, A.D. Pendergast, S. Goines, A.R. Bishop, A.T. Hoang, C. Renault, J.E. Dick, Nat. Commun. 10 (1) (2019) 1–8.
[9] W. Wang, JOM 66 (10) (2014) 2067–2077.
[10] J. Kim, H.S. Oh, J. Kim, C.W. Ryu, G.W. Lee, H.J. Chang, E.S. Park, Acta Mater. 155 (2018) 350–361.
[11] A. Cunliffe, J. Plummer, I. Figueroa, I. Todd, Intermetallics 23 (2012) 204–207.
[12] Y. Zhang, J.W. Qiao, P. Kliaw, J. Iron Steel Res. Int. 23 (1) (2016) 2–6.
[13] C. Fan, P.K. Liaw, C.T. Liu, Intermetallics 17 (1–2) (2009) 86–87.
[14] D. Ma, A.D. Stoica, X.L. Wang, Nat. Mater. 8 (1) (2009) 30–34.
[15] A.S. Argon, Acta Metall. 27 (1) (1979) 47–58.
[16] D.B. Miracle, T. Egami, K.M. Flores, K.F. Kelton, MRS Bull. 32 (8) (2007) 629–634.
[17] M. Yang, X.J. Liu, H.H. Ruan, Y. Wu, H. Wang, Z.P. Lu, J. Appl. Phys. 119 (2016) 245112.
[18] W. Li, H. Bei, Y. Tong, W. Dmowski, Y. Gao, Appl. Phys. Lett. 103 (17) (2013) 171910.
[19] J.C. Qiao, Q. Wang, J.M. Pelletier, H. Kato, R. Casalini, D. Crespo, E. Pineda, Y. Yao, Y. Yang, Prog. Mater. Sci. 104 (2019) 250–329.
[20] J. Brechtl, H. Wang, N. Kumar, T. Yang, Y.-.R. Lin, H. Bei, J. Neuefeind, W. Dmowski, S.J. Zinkle, J. Nucl. Mater. 526 (2019) 151771.
[21] J.T.M. De Hosson, Ultimi 192 (2018) 37–49.
[22] A. Takeuchi, N. Chen, T. Wada, Y. Yokoyama, H. Kato, A. Inoue, J.W. Yeh, Intermetallics 19 (10) (2011) 1546–1554.
[23] G. Rotter, H. Ishida, Macromolecules 25 (8) (1992) 2170–2176.
[24] H.B. Yu, W.H. Wang, K. Samwer, Mater. Today 16 (5) (2013) 183–191.
[25] H.B. Yu, K. Samwer, Y. Wu, W.H. Wang, Phys. Rev. Lett. 109 (9) (2012) 095508.
[26] H. Wagner, D. Bedorf, S. Küchemann, M. Schwabe, B. Zhang, W. Arnold, K. Samwer, Nat. Mater. 10 (6) (2011) 439–442.
[27] J.C. Ye, J. Lu, C.T. Liu, Q. Wang, Y. Yang, Nat. Mater. 9 (8) (2010) 619–623.

[28] Z. Wang, P. Wen, L.S. Huo, H.Y. Bai, W.H. Wang, Appl. Phys. Lett. 101 (12) (2012) 121906.
[29] T. Egami, J. Alloy Compd. 509 (2011) S82–S86.
[30] B. Wang, L. Luo, E. Guo, Y. Su, M. Wang, R.O. Ritchie, F. Dong, L. Wang, J. Guo, H. Fu, NPJ Comput. Mater. 4 (1) (2018) 1–11.
[31] P. Lunkenheimer, U. Schneider, R. Brand, A. Loid, Contemp. Phys. 41 (1) (2000) 15–36.
[32] T. Egami, S. Poon, Z. Zhang, V. Keppens, Phys. Rev. B 76 (2) (2007) 024203.
[33] D. Srolovitz, K. Maeda, V. Vitek, T. Egami, Philos. Mag. A 44 (4) (1981) 847–866.

[34] P. Gong, S. Zhao, H. Ding, K. Yao, X. Wang, J. Mater. Res. 30 (18) (2015) 2772–2782.
[35] Q. Zhou, Y. Du, W. Han, Y. Ren, H. Wang, Scr. Mater. 164 (2019) 121–125.
[36] J. Ma, C. Yang, X. Liu, B. Shang, Q. He, F. Li, T. Wang, D. Wei, X. Liang, X. Wu, Sci. Adv. 5 (11) (2019) eaax7256.
[37] J. Gu, M. Song, S. Ni, S. Guo, Y. He, Mater. Des. 47 (2013) 706–710.
[38] X. Wang, H. Lou, Y. Gong, U. Vainio, J. Jiang, J. Phys. – Condens. Mater. 23 (7) (2011) 075402.
[39] W. Li, Y. Gao, H. Bei, Sci. Rep. 5 (2015) 14786.